White Rose Research Online
eprints@whiterose.ac.uk
https://eprints.whiterose.ac.uk
Universities of Leeds, Sheffield and York

Deposited via The University of Sheffield.

White Rose Research Online URL for this paper:
https://eprints.whiterose.ac.uk/id/eprint/203251/

Version: Published Version

Article:
Do, H.-B., Luc, Q.-H., Pham, P.V. et al. (2023) Metal-induced trap states: the roles of interface and border traps in HfO2/InGaAs. Micromachines, 14 (8). 1606. ISSN: 2072-666X

https://doi.org/10.3390/mi14081606

Reuse
This article is distributed under the terms of the Creative Commons Attribution (CC BY) licence. This licence allows you to distribute, remix, tweak, and build upon the work, even commercially, as long as you credit the authors for the original work. More information and the full terms of the licence here: https://creativecommons.org/licenses/

Takedown
If you consider content in White Rose Research Online to be in breach of UK law, please notify us by emailing eprints@whiterose.ac.uk including the URL of the record and the reason for the withdrawal request.

Article

Metal-Induced Trap States: The Roles of Interface and Border Traps in HfO_2/InGaAs

Huy-Binh Do [1,*], Quang-Ho Luc [2], Phuong V. Pham [3], Anh-Vu Phan-Gia [1], Thanh-Son Nguyen [4], Hoang-Minh Le [5] and Maria Merlyne De Souza [6]

1 Faculty of Applied Science, Ho Chi Minh City University of Technology and Education, 01 Vo Van Ngan Street, Ho Chi Minh City 700000, Vietnam
2 Department of Materials Science and Engineering, National Yang Ming Chiao Tung University, 1001, Daxue Road, East District, Hsinchu 300093, Taiwan
3 Department of Physics, National Sun Yat-sen University, Kaohsiung 80424, Taiwan
4 Faculty of Fundamental Sciences, University of Architecture Ho Chi Minh City, 196 Pasteur St., Dist. 3, Ho Chi Minh City 700000, Vietnam
5 Faculty of electrical and electronics engineering, Ho Chi Minh City University of Technology and Education, 01 Vo Van Ngan Street, Ho Chi Minh City 700000, Vietnam
6 EEE Department, University of Sheffield, Sheffield S10 2TN, UK
* Correspondence: binhdh@hcmute.edu.vn

Abstract: By combining capacitance–voltage measurements, TCAD simulations, and X-ray photoelectron spectroscopy, the impact of the work function of the gate metals Ti, Mo, Pd, and Ni on the defects in bulk HfO_2 and at the HfO_2/InGaAs interfaces are studied. The oxidation at Ti/HfO_2 is found to create the highest density of interface and border traps, while a stable interface at the Mo/HfO_2 interface leads to the smallest density of traps in our sample. The extracted values of D_{it} of 1.27×10^{11} $eV^{-1}cm^{-2}$ for acceptor-like traps and 3.81×10^{11} $eV^{-1}cm^{-2}$ for donor-like traps are the lowest reported to date. The density and lifetimes of border traps in HfO_2 are examined using the Heiman function and strongly affect the hysteresis of capacitance–voltage curves. The results help systematically guide the choice of gate metal for InGaAs.

Keywords: defects in HfO_2; interface traps; border traps; acceptor-like and donor-like traps; Hf 4f peaks; valence band maximum; electronic band structure

Citation: Do, H.-B.; Luc, Q.-H.; Pham, P.V.; Phan-Gia, A.-V.; Nguyen, T.-S.; Le, H.-M.; De Souza, M.M. Metal-Induced Trap States: The Roles of Interface and Border Traps in HfO_2/InGaAs. *Micromachines* **2023**, *14*, 1606. https://doi.org/10.3390/mi14081606

Academic Editors: Xiao Luo, Bo Yao and Parsian K. Mohseni

Received: 16 May 2023
Revised: 1 August 2023
Accepted: 11 August 2023
Published: 15 August 2023

Copyright: © 2023 by the authors. Licensee MDPI, Basel, Switzerland. This article is an open access article distributed under the terms and conditions of the Creative Commons Attribution (CC BY) license (https://creativecommons.org/licenses/by/4.0/).

1. Introduction

Hf-based high-k oxides (Hf-based ferroelectrics) have been identified as one of the most promising candidates in future microelectronic applications [1–7] due to their excellent compatibility with existing Complementary Metal Oxide Semiconductor (CMOS) processes [8–13]. The functional properties of HfO_2 depend critically on its defects: oxygen vacancies [14] or the metal/HfO_2 [15] and HfO_2/substrate [3] interfaces. A low density of oxygen vacancies is required as dielectric for low power-consumption devices [2,3], whereas high density is attractive in ferroelectric FETs and resistive random access memory (ReRAM) [16–18]. The conductivity of HfO_2-based materials is believed to be governed by oxygen vacancies via the formation of a conducting filament [19,20]. A change in local band structure [21], oxygen vacancy-induced trap states [22], conducting oxide [23], and crystalline suboxide phases [24] all contribute to explaining the conductivity of HfO_2-based materials.

Among III-V materials, InGaAs is a promising epitaxial layer due to its high electron mobility and small band gap of 0.74 eV [25] in high-speed and low-power logic technologies [26–29]. InGaAs quantum well metal oxide semiconductor field effect transistors (MOSFETs) with a gate length of 70 nm were shown to yield a current gain of ~1×10^4 by J. Lin et al. [26]. X. Cai et al. reported that a high mobility of 570 cm^2/V·s can be reached

in InGaAs FinFETs at a fin width of 7 nm. Gate oxide trapping was believed to degrade the device's performance [27]. In logic applications, InGaAs gate-all-around MOSFETs with sub-10 nm top-width nanowires were investigated with the subthreshold voltage of 70 mV/dec [28]. Unlike a favorable Si/SiO_2 interface in silicon, there is a lack of native oxide in InGaAs, leading to techniques in plasma treatment of the surface [2], passivation using sub-nanometer AlN [30], and chemical treatment [31] to achieve interface engineering. This approach is based on the effect of the InGaAs epitaxial layer on the properties of HfO_2 layers. However, gate metals may also induce trap states at the metal/HfO_2 interface [15], facilitating the diffusion of the oxygen vacancy in HfO_2 films. The passivation of the metal/HfO_2 interface was conducted using the AlN layer [4], resulting in an increase in the permittivity of HfO_2 of 47%. Studies of bias temperature instability revealed the role of deep states in high-k to degradation [32]. Although there are many studies of interface traps at HfO_2/InGaAs arising from the interaction between HfO_2 and the InGaAs layer, the behavior of interface traps and border traps due to the effects of gate metals have not been systematically examined. Studying these effects is required not only in logic but also resistive random-access memory (RRAM) devices.

To answer the questions raised by a metal-induced interface and border traps in HfO_2 and at the HfO_2/InGaAs interfaces, the electrical properties of HfO_2 in metal/HfO_2/InGaAs structure are investigated in this study using metal oxide semiconductor capacitors (MOSCAPs). A TCAD simulation is adapted to simulate electrical characteristics and the band structure of devices. The properties of interface traps and border traps are extracted from a comparison of the theoretical capacitance–voltage (CV) characteristics and experiments. The material properties of HfO_2 are investigated using transmission electron microscopy (TEM) and X-ray photoelectron spectroscopy (XPS) spectra. Based on material and electrical investigations, we explain systematically the role of gate metals in the formation of acceptor-like and donor-like traps at the HfO_2/InGaAs interface, as well as the border traps within HfO_2.

2. Experimental Procedure and TCAD Simulation

2.1. Experimental Procedure

$In_{0.53}Ga_{0.47}As$ (IGA) MOSCAPs were fabricated following the process flow shown in Figure 1a. The channel layer is a commercial 100 nm n-doped $In_{0.53}Ga_{0.47}As$ (5.0×10^{17} cm^{-3} Si-doped) layer grown on n+-InP substrate by solid source molecular beam epitaxy. Acetone (ACE) and isopropanol (IPA) were used to clean the IGA surface before the native oxide was etched in dilute HCl. The samples were subsequently loaded into an ALD chamber for the deposition of high-k with a growth temperature of 250 °C. The deposition process includes 2 steps: (i) 5 cycles of the AlN layer with a thickness of ~0.7 nm, as shown in Figure 1b, and (ii) HfO_2 layers, in which the thicknesses varied from 50 cycles to 150 cycles. The growth rate of HfO_2 was determined to be ~0.73 Å/cycle, as shown in Figure 1c. All of the thicknesses of HfO_2 were measured and fitted using a SOPRA GES5 Ellipsometer because of the large number of samples. Thicknesses of 50 cycles of HfO_2 samples are double checked using the HRTEM. Post-deposition anneal (PDA) was conducted at 450 °C for 2 min in forming gas (FG) after the high-k deposition. The HRTEM in Figure 1b indicates that the atomically sharp and clear Ni/HfO_2/AlON/$In_{0.53}Ga_{0.47}As$ interface of the PDA sample was obtained with virtually no interdiffusion. HfO_2 film was found to be amorphous in Figure 1b, which is in agreement with the report [33]. Finally, a contact was defined on HfO_2 via lithography/lift-off processes, followed by a post-metallization anneal at 250 °C for 30 s in FG.

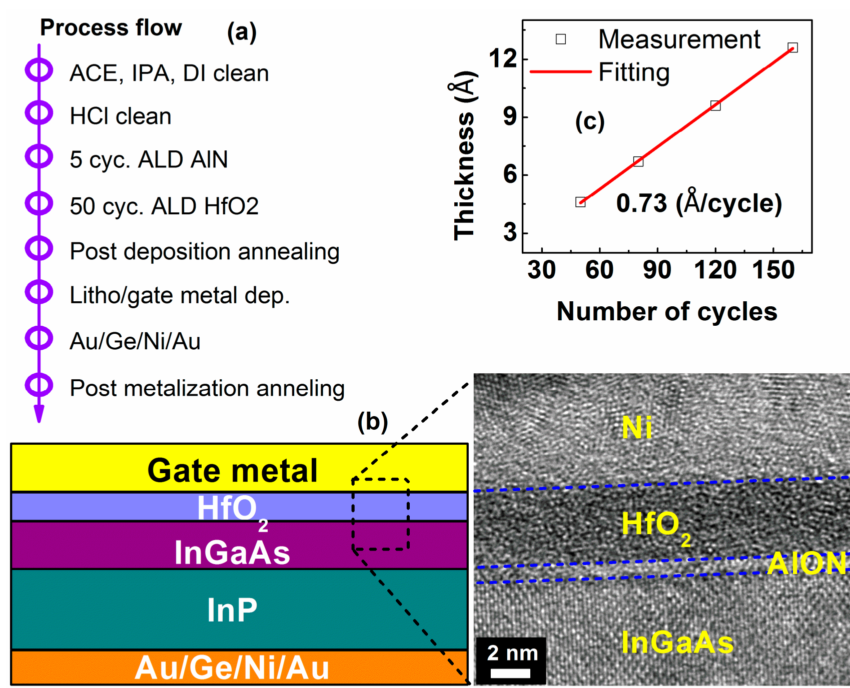

Figure 1. (**a**) Process of fabrication of $HfO_2/In_{0.53}Ga_{0.47}As$ MOSCAPs. (**b**) The schematic cross-section and HRTEM image of the metal/$HfO_2/In_{0.53}Ga_{0.47}As$ structure after PDA. (**c**) The relationship between HfO_2 thickness and the number of cycles in the ALD chamber. The growth rate was determined at ~0.73 Å/cycle.

2.2. Simulation of CV Characteristics

HfO_2/IGA MOSCAPs were simulated using the Silvaco TCAD 2-D device simulation tool. The flowchart of the process simulation is shown in Figure S1 in the supporting information. The structure of the MOSCAPs is illustrated in Figure 1b. To consider the effects of the high field on mobility and carrier concentration on carrier lifetime, a high field model and a concentration-dependent lifetime model were adopted, respectively. The Auger recombination model was utilized to account for the effect of high electron concentration (N_e). The Shockley–Read–Hall model was used to simulate the trap-assisted recombination. The band gap narrowing effect was included in the simulation to consider a shrinkage of the bandgap occurring when the impurity concentration is particularly high. To make sure that the models being used represent and replicate a real-world device accurately, TCAD parameters (shown in Table 1) were calibrated against the device structure in Figure 1b through capacitance–voltage (CV) characteristics. The electron affinity of HfO_2 was used based on the extracted valence band offset of the HfO_2/IGA heterostructure from XPS measurements, and the permittivity of HfO_2, corresponding to different gate metals, were extracted from the curve of measured capacitance-equivalent thickness (CET) versus HfO_2 thickness. The parameters of IGA are default values from Silvaco TCAD.

Table 1. Parameters used in HfO_2/IGA MOSCAPs.

Material Parameters	HfO_2	AlON	$In_{0.53}Ga_{0.47}As$ [1]
Band gap (eV)	5.7 [34]	7 [34]	0.734
Electron affinity (eV)	2.52 [2]	0.88 [2]	4.67
Permittivity	10.9–21 [3]	8.8 [34]	13.9
Effective density of state in the conduction band (cm^{-3})	-	-	2.1×10^{17}
Effective density of state in the valence band (cm^{-3})	-	-	7.7×10^{18}
Intrinsic carrier concentration (cm^{-3})	-	-	8.72×10^{11}
Electron mobility ($cm^2/V \cdot s$)	-	-	10^4
Effective electron mass	-	-	$0.041\ m_o$
Effective hole mass			$0.46\ m_o$
Tunnelling effective masses	$0.17\ m_o$ [35]	$0.35\ m_o$ [35]	-
Saturated electron drift velocity (cm/s)	-	-	2.5×10^7
Saturated hole drift velocity (cm/s)	-	-	7.7×10^6

[1] Parameters of InGaAs are default values from TCAD. [2] Based on the band offset of HfO_2/InGaAs, extracted from XPS spectra. [3] Values extracted from CET thickness curves.

3. Results and Discussion

3.1. Experimental Electrical Behavior

Figure 2 shows multi-frequency (1 kHz–1 MHz) C-V characteristics with different gate metals whose work functions are 4.33 eV (Ti), 4.95 eV (Mo), 5.10 eV (Pd), and 5.15 eV (Ni) [36]. It is seen that except for sample A, all other samples provide quite similar C-V characteristics. The high-frequency dispersion in the accumulation of sample A is due to high densities of border traps in the bulk of the dielectric [37,38]. Samples A, C, and D exhibit typical 'humps' around 0 V of some C-V curves, indicating the presence of interface traps, which can be suppressed effectively by increasing the frequency [39]. The minimal frequency dispersion of the accumulation capacitance in sample D and the smallest hump around 0 V in sample B qualitatively indicate that Ni and Pd gate metals induce small densities of interface (D_{it}) and border traps (N_{BT}). The effects of gate metals on the interface and border traps are going to be analyzed in the simulation section. At 1 kHz, a high inversion capacitance equal to the oxide capacitance (C_{ox}) in sample B indicates that minority carriers respond freely to the signal to form a fully inverted layer in agreement with previous reports [40].

Figure 3a shows the capacitance oxide thickness (CET) at +2 V and 1 MHz versus the HfO_2 thickness (t_{HfO2}) curves of all samples. The total thickness of HfO_2 and AlON in this study is large enough to neglect the quantum effect [41]. The charge centroid is expected to be at the AlON/InGaAs interface when identifying the thickness of the oxide in accumulation. CET is a function of the HfO_2 thickness (t_{HfO_2}) following Equation (1).

$$CET = \frac{\varepsilon_{SiO_2}}{\varepsilon_{HfO_2}} t_{HfO_2} + \frac{\varepsilon_{SiO_2}}{\varepsilon_{AlON}} t_{AlON} + \varepsilon_{ox} \frac{\partial(\Psi_s - \Psi_{s,G})}{\partial(D_s)} \quad (1)$$

where ε_{HfO_2} and t_{AlON} are the permittivity of the HfO_2 and the thickness of *AlON*, respectively, $\varepsilon_{SiO_2} = 3.9$, Ψ_S and $\Psi_{S,G}$ are the band bending at the channel and gate electrodes, respectively, and D_S is the electric displacement in the substrate just beneath the oxide/InGaAs interface. Equation (1) allows the permittivity of the high-k layer to be extracted based on the slopes of the CET-t_{ox} curves in Figure 3a, without knowing the band bending at the channel and gate electrodes. The extracted values of permittivity are shown in Figure 3b. The values of permittivity of the Ti-, Mo-, and Ni-gated samples are the same, fluctuating around 18.5 to 21, which is in agreement with a previous report [42]. The permittivity of the Pd sample is ~11, too small to compare to others, which is likely due to the formation of a PdO layer [15] with a small permittivity of ~8 [43].

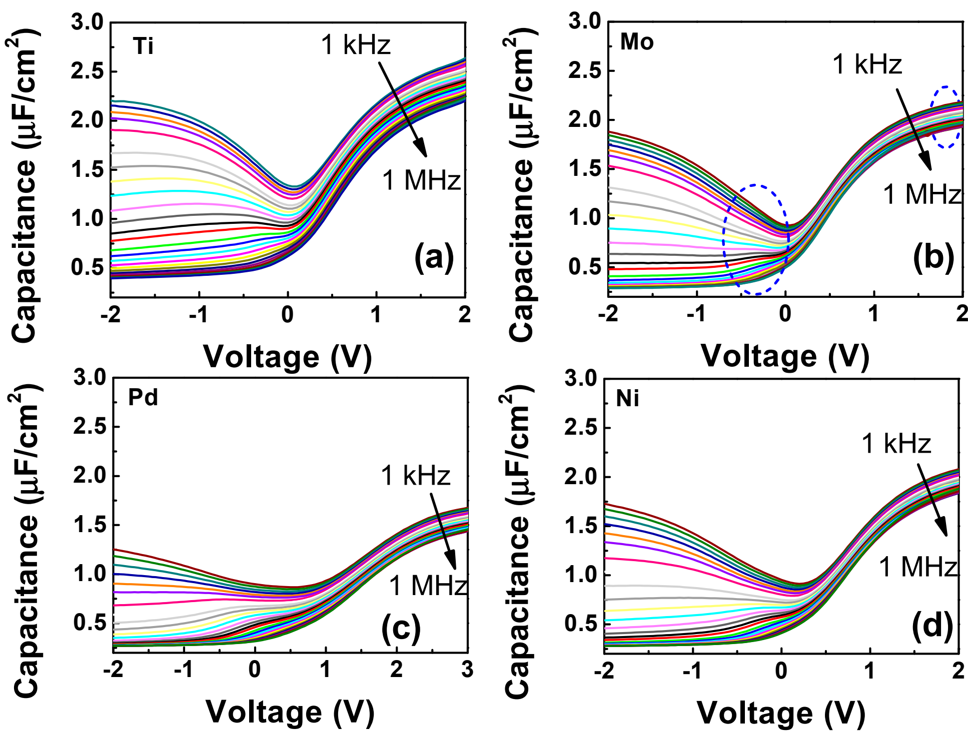

Figure 2. Multi-frequency (1 kHz–1 MHz) C-V characteristics of MOSCAPs with different gate metals: (**a**) Ti, (**b**) Mo, (**c**) Pd, and (**d**) Ni. A hump around 0 V and high C-V dispersion is found in the Ti sample, indicating the presence of high densities of interface (D_{it}) and border traps (N_{BT}). Oppositely, the lowest capacitance is in the Pd sample, referring to the degradation of permittivity of HfO_2 when Pd is used as a gate metal. The best C-V behavior without hump around 0 V and small C-V dispersion is in the Mo sample (highlighted by blue circles), implying the lowest D_{it} and N_{BT}.

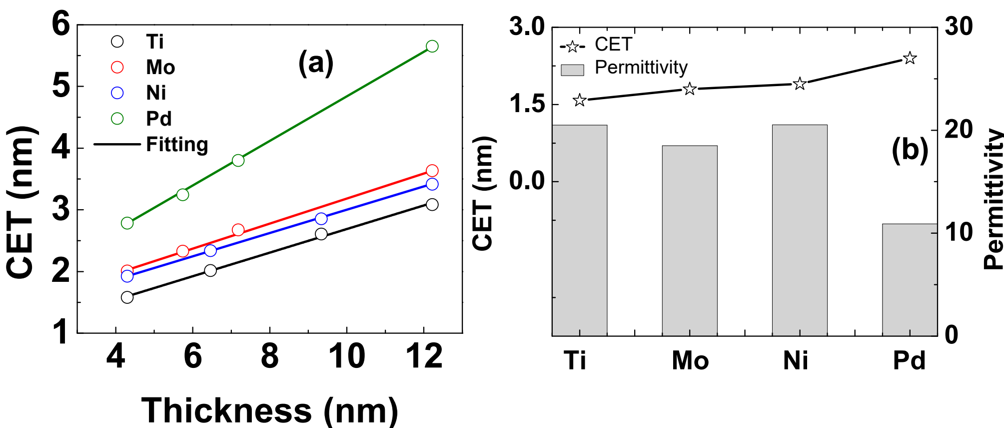

Figure 3. (**a**) Equivalent capacitance thickness (CET) versus physical oxide thickness of all samples. (**b**) Equivalent capacitance thickness (CET) and permittivity of all samples for a physical oxide thickness of 4.3 nm.

3.2. Effects of Gate Metals on Interface Traps and Border Traps

The impact of fast and slow traps on the electrical properties of HfO_2 on IGA is examined via TCAD simulations using the parameters shown in Table 1. Interface and border traps are included at the AlON/IGA interface and within the band gap of HfO_2 (for example, oxygen vacancies), respectively, to fit the simulation C-V curves to the ones observed in the experiment. The effects of the AlON/HfO_2 interface traps on C-V curves are not separately investigated in this study because it is hard to distinguish this type of trap from others. Instead, this trap and border trap are considered as a single object.

Additionally, a negative interface fixed charge of around 5.0×10^{11} cm^{-2} to 1.5×10^{12} cm^{-2}, similar to that in a recent study, is included [44]. The interface fixed charges are related to the incorporation of nitrogen in high-k dielectrics during ALD deposition or in post-deposition treatment [45,46]. This charge is treated as a sheet of charge at the interface controlled by the interface boundary condition, which causes the shift of the C-V curves. On the other hand, interface traps and bulk traps are added as space charge directly into the right-hand side of Poisson's equation:

$$div(\varepsilon \nabla \Psi) = -\rho = q\left(n - p - N_D^+ + N_A^-\right) - Q_T \quad (2)$$

where Ψ is the electrostatic potential, ε is the permittivity, ρ is the local space charge density, N_D^+ and N_A^- are the ionized donor and acceptor impurity concentrations, respectively, and Q_T is the charge due to traps and defects. The total charge caused by the presence of traps in the right-hand side of Poisson's equation can be defined by:

$$Q_T = q\left(N_{tD}^+ - N_{tA}^-\right) \quad (3)$$

where N_{tD}^+ and N_{tA}^- are the densities of the ionized donor-like and acceptor-like traps, respectively.

It is seen in Figure 4a–d that the simulation results fit well with the experiment. The process to calibrate the simulation curves consists of two steps: (i) adding interface traps to the AlON/IGA interface to fit C-V curves in the forward bias and (ii) simulating C-V curves in reverse bias to obtain hysteresis by adding border traps in the bandgap of HfO_2. There are two types of interface traps: donor-like and acceptor-like. A donor-like trap can be either positive or neutral, and it is positively charged (ionized) as empty and neutral as filled (with an electron). An acceptor-like trap can be either negative or neutral, and it is neutral as empty and negatively charged (ionized) as filled (with an electron). One of the well-known methods to extract densities of interface traps (D_{it}) is the conductance method. This method is based on estimating the peak of equivalent parallel conductances calculated from measured impedance [47]. The advantage of this method is that the D_{it} can be extracted directly from experimental data. However, the extracted D_{it} is reported to be not correct in the case of large D_{it}, especially when $C_{ox} < qD_{it}$ [47]. Another popular method is the Terman method. To extract D_{it}, the ideal C-V curve is plotted. The stretch-out of the experimental curve as compared to the ideal one provides the value of D_{it}. The D_{it} extracted by the Terman method is typically larger (~10 times) than that extracted by the conductance method [4].

Figure 4e shows the D_{it} of all samples extracted from TCAD simulations. It is seen that D_{it} is minimal at the mid gap, and acceptor-like densities are smaller as compared to donor-like densities for all samples. The lifetime of interface traps is extracted to be 2.9×10^{-9} s, which is the same as the previous study [48]. The smallest D_{it} (1.39×10^{11} eV^{-1}cm^{-2} acceptor-like traps, and 3.81×10^{11} eV^{-1}cm^{-2} donor-like traps) is in the sample with a Mo gate. This result is in accordance with the multi-frequency C-V curves in Figure 2b, where the Mo sample seems to not present any hump around 0 V at high frequency. In contrast, the highest D_{it} is in the Ti-gated sample, corresponding to the largest hump around 0 V at a high frequency, as shown in Figure 2a. The fact that the D_{it} from donor-like traps near the valence band edge of all samples is much smaller compared to those near the conduction band edge confirms the strong inversion of the multi-frequency C-V curves of all samples shown in Figure 2, implying freely moving minority carriers in the channel. In our previous report, a combination of Mo/Ti gate metal and the passivation layer AlN between Ti and HfO_2 leads to a small D_{it} [4]. In that study, a thin AlN layer was believed to prevent the reaction between Ti and HfO_2, diminishing the formation of oxygen vacancies in HfO_2.

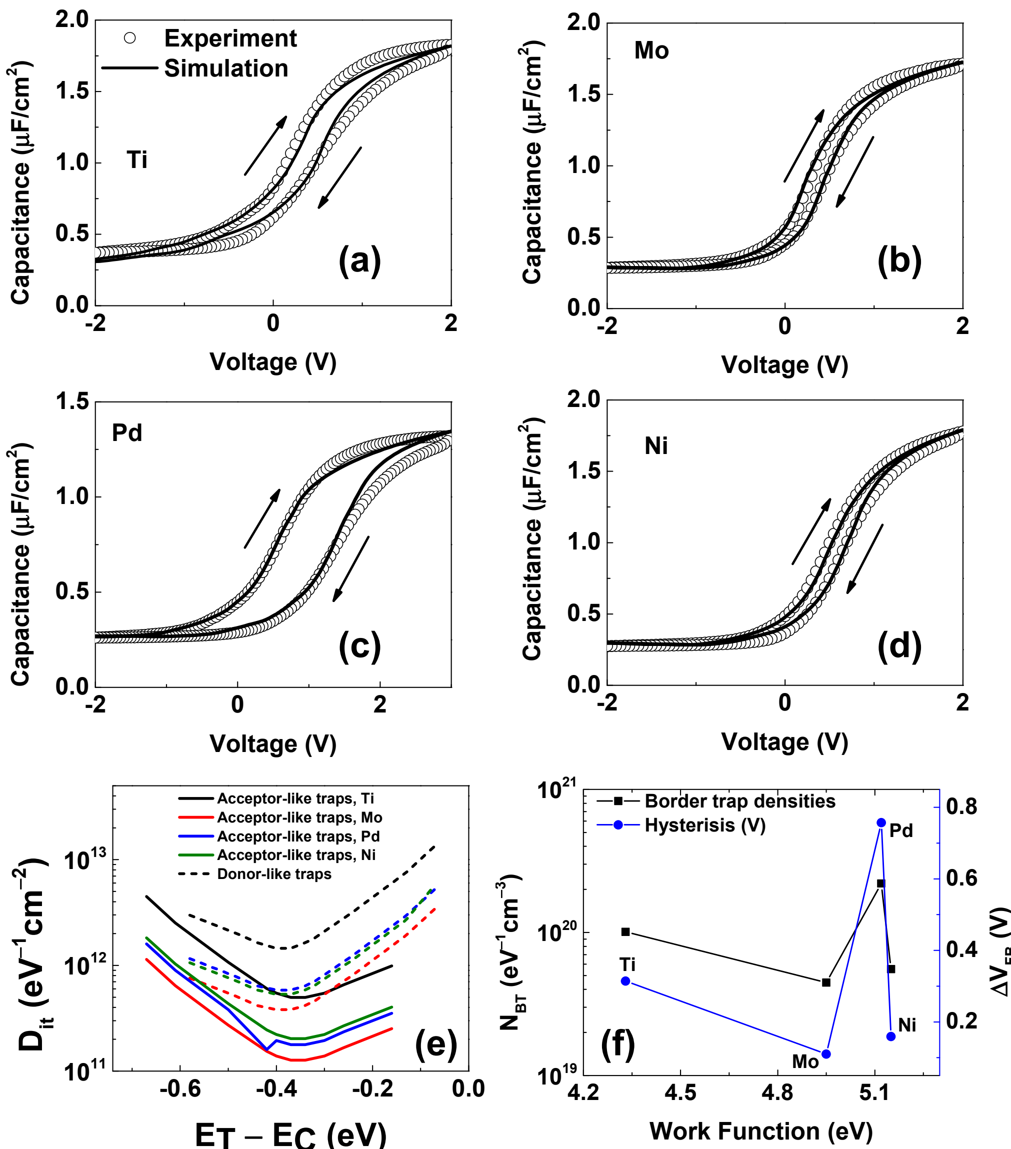

Figure 4. Results of C-V characteristics at 1 MHz from TCAD simulations and experiment of (**a**) Ti, (**b**) Mo (**c**) Pd, and (**d**) Ni samples. The up and down arrows illustrate the forward and reverse sweep of C-V curves, respectively. (**e**) Densities of interface traps extracted from TCAD simulations of the C-V curves in (**a**–**d**). (**f**) The densities of border traps and the difference in flat band voltage of the samples are shown in (**a**–**d**).

The extracted border traps are shown In Figure 4f. Because the border traps near the conduction band strongly affect the n-type substrate, only acceptor-like border traps are considered in this study [49]. To simulate the hysteresis of C-V curves, the Heiman method [50] is utilized. The traps are assumed to have a uniform distribution with depth in HfO_2, but the capture cross-section σ_{nx} and the lifetime of traps τ_T for electrons are a function of distance from the AlON/IGA interface:

$$\sigma_{nx} = \sigma_n e^{-2k_e x} \tag{4}$$

$$\tau_T = \frac{1}{n_s \overline{v} \sigma_{nx}} \tag{5}$$

where x is the distance from the interface to the trap position in HfO_2, σ_n is the capture cross-section of traps for electrons at the interface, n_s is the trap concentration at the interface, $\overline{v}$ is the thermal velocity of electrons, and k_e is determined from:

$$k_e^2 = \frac{2m_e^*(E_C - E_{tA})}{\hbar^2} \quad (6)$$

where E_C, m^*_e, E_{tA}, $\hbar$, and E_{tA} are the conduction band minimum, the effective mass of the electron, the border trap level, the Planck constant, and the level of the acceptor-like trap, respectively. It is seen that the largest border traps of 2.2×10^{20} $eV^{-1}cm^{-3}$ occur in the Pd sample, explaining the largest hysteresis of 0.76 V of CV curves in Figure 4c. The extracted lifetime of border traps at the interface is 2.5×10^{-5} s, which is larger than the interface traps. The value of lifetime is the same as in the study of Zhang et al. [51]. For the border traps in high-k, the values of lifetimes are calculated in Equation (5). Similar to the extracted D_{it}, the smallest value of border traps, an N_{BT} of 4.46×10^{19} $eV^{-1}cm^{-3}$, also occurs in the Mo sample, which is confirmed by the smallest hysteresis in its C-V hysteresis of 0.11 V, as shown in Figure 4f. Although the work function of Ni and Pd is nearly the same, the quality of the Ni sample is much better than Pd. The reasons for the degradation have been discussed in our previous report, where the formation energy of the metal oxygen defect has a critical role that stabilizes the metal/high-k interface [15].

The effects of D_{it} and N_{BT} are systematically studied in Figure 5. Figure 5a indicates that the ionization profiles of interface traps extracted from the TCAD simulation depend on the types of traps and their positions as compared to the charge neutrality level (CNL) at 0.21 eV inside the IGA band gap [52]. It is seen that donor-like traps are ionized above CNL, creating a positive charge at the interface. A complete ionization of the interface of donor-like traps generates a net positive charge, contributing to the total capacitance, which induces a negative shift and up-shift of C-V curves (pink solid line) compared to the ideal (black solid line) at a negative voltage, as shown in Figure 5b. Based on the stretch-out of C-V curves due to these shifts, it was reported that densities of interface traps could be extracted by the Terman method [47]. However, in our case, it was impossible to separate the densities of ionized and neutral traps using this method. Opposite to donor-like traps, acceptor-like traps are filled below the CNL, as shown in Figure 5a. These traps induce a net negative charge at the interface, the same as the interface-fixed charge, when they are completely ionized. These traps also cause a right shift of the C-V curve and a decrease in the accumulation capacitance, as shown in Figure 5b (pink solid line). To distinguish the effects of donor-like and acceptor-like traps on the charge density of the channel below HfO_2, donor-like traps (D_{it} = 3.81×10^{11} $eV^{-1}cm^{-2}$) or acceptor-like traps (D_{it} = 1.27×10^{11} $eV^{-1}cm^{-2}$) are added at the mid gap of the Mo sample in our C-V simulation. It is clear that single donor-like traps shift the C-V curves up around 0 V (red dash line). This shift means that a hump around 0 V can be created when the D_{it} of donor-like traps is high and the measured frequency is small, as seen in the experiment in Figure 2a,c,d. The blue dashed line in Figure 5b illustrates that acceptor-like traps act as a sheet of a negative fixed charge and shift the C-V curves to positive voltage. The effect of the density of border traps on the C-V curves of the Mo sample is shown in Figure 5c. In all simulations, border traps are assumed to distribute in the dielectric with a maximum depth of 2 nm from the interface, and the continuously distributed states are represented by 20 discrete trap states along a depth of 2 nm, as shown in Figure 6a. It is seen that there is no C-V hysteresis when N_{BT} = 4.47×10^{18} $eV^{-1}cm^{-3}$. The change in the order of N_{BT} causes a significant variation of the hysteresis, and the hysteresis larger than 1.0 V is found as N_{BT} = 4.47×10^{20} cm^{-3}. The impact of a lifetime of border traps is considered in Figure 5d. Because only acceptor-like border traps near the conduction band edge are investigated, the lifetime affects meaningfully the accumulation region. Since the simulated frequency is 1 MHz, a lifetime of 2.9×10^{-3} s induces no consequence on C-V curves. The border traps have a substantial response if they have a lifetime smaller than 2.9×10^{-5} s, which is in agreement with the literature [51].

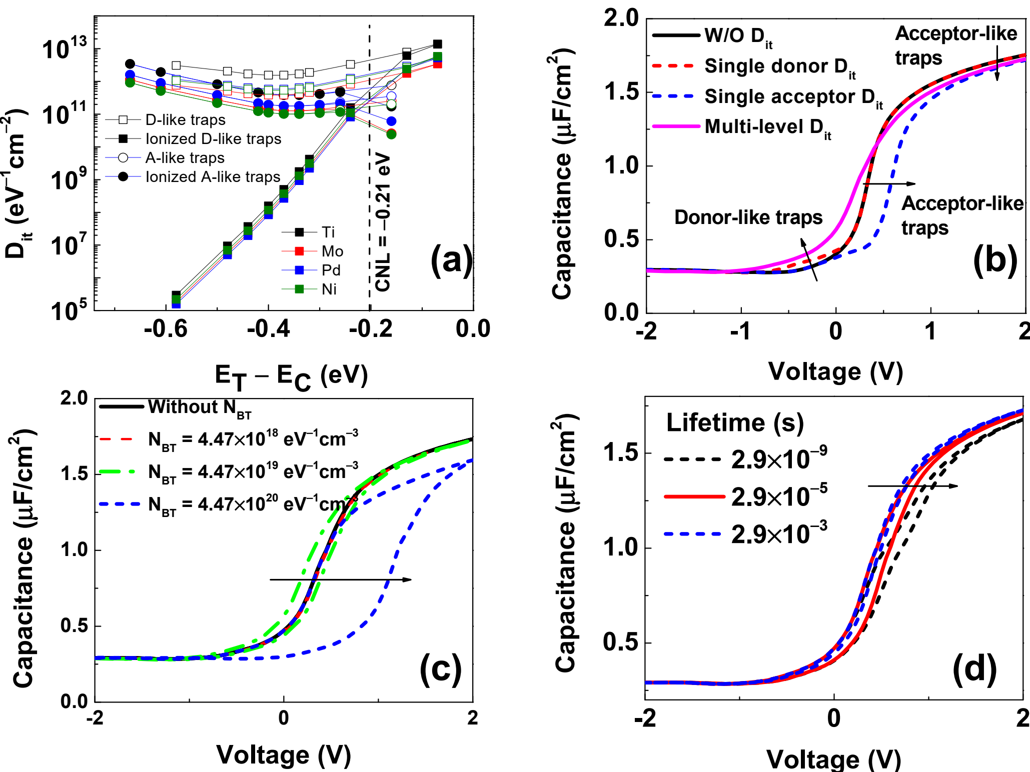

Figure 5. (**a**) The distribution of ionized donor-like and acceptor-like traps at the AlON/InGaAs interface. Trap positions are compared with the conduction band minimum of InGaAs. (**b**) Effects of the kinds of interface traps on the C-V behaviors. Impacts of (**c**) densities and (**d**) lifetime of border traps on the C-V behaviors. The black arrows highlight the shift of C-V curves under the effects of interface traps, border traps, and the lifetime of traps.

3.3. Properties of Metal/HfO$_2$/AlON/In$_{0.53}$Ga$_{0.47}$As Structures

Band diagrams of all samples were extracted from the TCAD simulation at 0V, as shown in Figure 6a. The simulated band offsets of the HfO_2/AlON/IGA structures were compared with data from XPS measurements, as shown in Figure 6b. The band offsets of the AlON/IGA and HfO_2/AlON structures are extracted to be 2.47 eV and 0.35 eV, respectively, showing agreement between the experiment and simulation. Although five cycles of the AlN layer were deposited on IGA for passivation, XPS revealed that this layer was AlON [3]. It is found that low and high work function gate metals induce opposite bending in the band diagram. This bending depends on the flat band voltage described by [53]:

$$V_{FB} = \varphi_{\text{m,eff}} - \varphi_S - \left(Q_f \frac{\varepsilon_{SiO_2}}{\varepsilon_{ox}^2} t_{ox} + \frac{1}{2} \rho_{ox} \frac{\varepsilon_{SiO_2}}{\varepsilon_{ox}^2} t_{ox}^2 \right) \quad (7)$$

where V_{FB} is the flat band voltage, ϕ_{m} is the work function of metals, ϕ_{S} is the semiconductor work function, Q_f is the interface fixed charges, ε_{SiO2} is the permittivity of SiO_2, ε_{ox} is the permittivity of HfO_2, t_{ox} is its thickness, and ρ_{ox} is bulk HfO_2 charge density. The relationship between V_{FB} and tox was reported to be linear in the HfO_2/IGA moscap, so the effect of ρ_{ox} on V_{FB} is much smaller compared to Q_f on V_{FB} [3]. Because the density of interface fixed charge used to calibrate the C-V curves is quite similar ~10^{12} cm^{-2} in all samples, bending in the band diagram should be from the difference in metal work functions and the bulk charges shown in Figure 4f alone. Additionally, the border acceptor-like traps studied in this work are empty at 0 V, as shown in Figure 4f, referring to its neutral state at 0 V above the CNL. These trap charges also need a delay time to fill up. The opposite band bending (0.62 eV–0.89 eV) of the samples shown in Figure 6a is in agreement with the C-V curves in Figure 4a–d, illustrating a negative C-V shift of the Ti sample and a positive C-V

shift of the others. This bend bending is also confirmed by the valence band maxima of XPS spectra measured at metal/HfO_2 interfaces, as shown in Figure 6c.

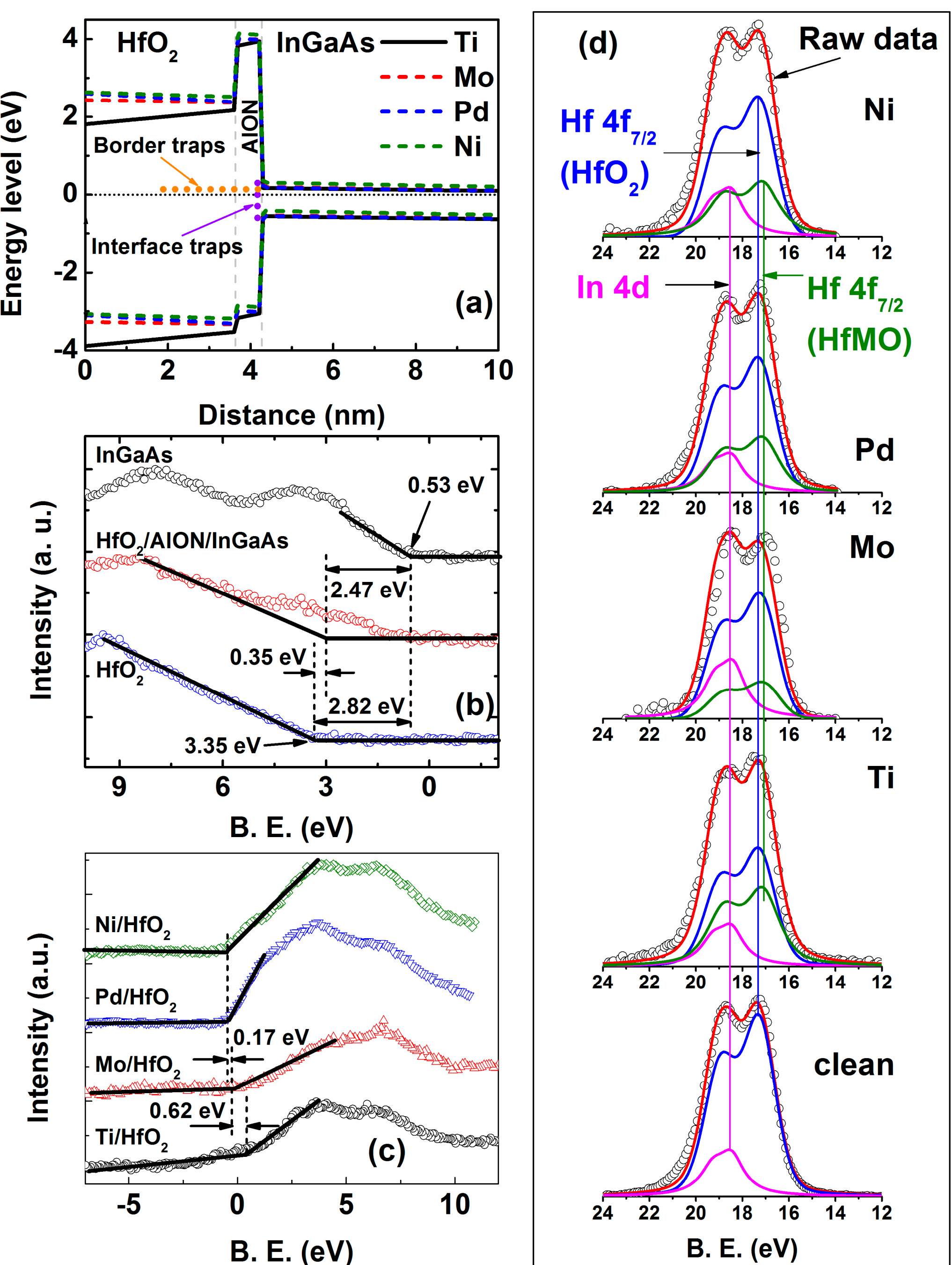

Figure 6. (**a**) Band diagram of a metal/HfO_2/AlON/InGaAs structure extracted by TCAD simulation. (**b**) Valence band maxima of an HfO_2/AlON/IGA structure derived from XPS measurement. (**c**) Valence band maxima of metal/HfO_2 structures derived from XPS measurement. (**d**) Hf $4f_{7/2}$ of clean HfO_2 surface and (Ti, Mo, Pd, Ni)/HfO_2 interfaces.

To analyze the interaction of the metal/HfO_2 interface, the factor that most impacts D_{it} and N_{BT} is the convolution of the Hf 4f peaks shown in Figure 6d. All samples with a diameter of ~5 mm were mounted on an XPS holder using copper tape. The pressure of the XPS chamber is ~10^{-9} torr when the measurement was conducted. For the analysis, the core levels were determined by using XPSPEAK with a Gaussian–Lorentz line shape and Shirley background, with an uncertainty of the core position of 0.05 eV. Sample charging

effects were corrected by placing the C 1s peak at a binding energy (BE) of 284.8 eV and shifting the rest of the regions accordingly. The binding energy, the spin–orbit splitting (SOS), and the full-width at half-maxima (FWHM) values used to fit the curves of the two samples are shown in Table 2. For the clean HfO_2 sample, there are two peaks that are convoluted: an Hf $4f_{7/2}$ peak at 17.12 eV [3,54] and an In 4d peak at 18.47 eV [3,55], representing the In-O bond. The presence of an In peak with an area of ~10% is believed to be due to In diffusion from the InGaAs layer [55]. In the other samples, Hf $4f_{7/2}$ peaks were split into three peaks. One of them is the Hf $4f_{7/2}$, which appears in the clean HfO_2 sample, denoted as a peak of deposited HfO_2. The In-O peak in other samples was kept to have the same BE, SOS, FWHM, and area to ensure that it does not affect other peaks in the fitting process. It is seen that a new peak at 16.97 eV dominates in all samples (besides the peak of Hf $4f_{7/2}$), except in clean HfO_2. The BE of this peak is in a range of the Hf $4f_{7/2}$ peak (from 14.3 eV for Hf metal to 18.3 eV for perfect HfO_2 oxide) [56], so it can be inferred that gate metals react with the oxygen in HfO_2, producing a complex interface that contains HfMO (M: Ti, Mo, Pd, and Ni). We denote Hf $4f_{7/2}$ in clean HfO_2 and HfMO as Hf1 and Hf2 peaks, respectively. The area ratio of Hf2 and Hf1 peaks, A_{Hf2}/A_{Hf1}, should give us information relating to the oxidation of the gate metals because more oxidation causes a higher intensity of the Hf2 peak. The area ratios A_{Hf2}/A_{Hf1} in the Ti, Mo, Pd, and Ni samples were extracted at 0.775, 0.296, 0.460, and 0.390, respectively, implying that the the Mo sample created the most stable interface on HfO_2. Its XPS result is in agreement with its C-V behavior shown in Figure 2b, with the lowest values of D_{it} and N_{BT} shown in Figure 4e,f. The stability of the Mo/HfO_2 and Ni/HfO_2 interfaces is also confirmed in the TEM measurement shown in Figure S2b,d (supporting information). Oppositely, the Ti/HfO_2 interface has the highest ratio, A_{Hf2}/A_{Hf1}, indicating a strong reaction between Ti and O_2^- in HfO_2. This reaction is observed in Figure S2a (supporting information), showing the increase in roughness at the Ti/HfO_2 interface. This reaction can be suppressed by passivating the HfO_2 surface using an ultra-thin AlN layer, which was reported in our previous work [4]. The area ratio A_{Hf2}/A_{Hf1} in the Pd sample is slightly higher than the Ni sample, indicating that Pd-O facilitates oxidation at the AlON/IGA interface due to the transportation of oxygen vacancies in HfO_2. Yoshida et al. reported that Pd-O induced a thin In-O layer between HfO_2 and IGA [57]. The effect of Pd-O on the HfO_2 layer should be similar to this study. However, the TEM image in Figure S2c does not show the In-O layer. Instead, Pd-O causes the defects in the AlON layer, illustrated by the white arrows in Figure S2c, supporting information. The difference in the formation of the In-O layer at the high-k/IGA interface is due to the fact that AlON is an excellent passivation layer [1]. The results indicate that the reaction at the metal/HfO_2 interface is the main factor that creates an oxygen vacancy in HfO_2, contributing to high D_{it} at the HfO_2/IGA interface and high N_{BT} in bulk HfO_2. The high value of N_{BT} is a disadvantage in devices for logic applications but an advantage in memory devices.

Table 2. BE, SOS, and equal FWHM values were applied to fit the curves in Figure 6d (eV).

	Hf $4f_{7/2}$ (Clean HfO_2)	**In-O**	**Hf $4f_{7/2}$ (HfMO), M = Ti, Mo, Pd, Ni**
BE (eV)	17.12	18.47	16.97
SOS (eV)	1.68	0.8	1.68
FWHM	1.62	1.28	1.68

Figure 7 shows the leakage current through HfO_2. These currents can be described by the tunneling effects in the Fowler–Nordheim regime [58]:

$$J_t = \frac{J_0}{\Phi_B} E_{ox}^2 exp\left(-\frac{k\Phi_B^{3/2}}{E_{ox}}\right) \quad (8)$$

J

where Φ_B and E_{ox} represent the tunneling barrier and oxide electric field, respectively. It is clear that the Ti sample has high leakage current shown in Figure 7a due to the lower barrier of the AlON layer shown in Figure 6a and the high value of high D_{it} and N_{BT} shown in Figure 4e,f. Oppositely, the Mo and Ni samples have the lowest leakage current. These two samples have the same band bending shown in Figure 7a and the low D_{it} and N_{BT} shown in Figure 4e,f. For logic applications, D_{it} can be benchmarked as a function of CET, as shown in Figure 7b. Our extracted value is revealed to be the smallest (1×10^{11} $eV^{-1}cm^{-2}$ for acceptor-like traps) compared to other reports.

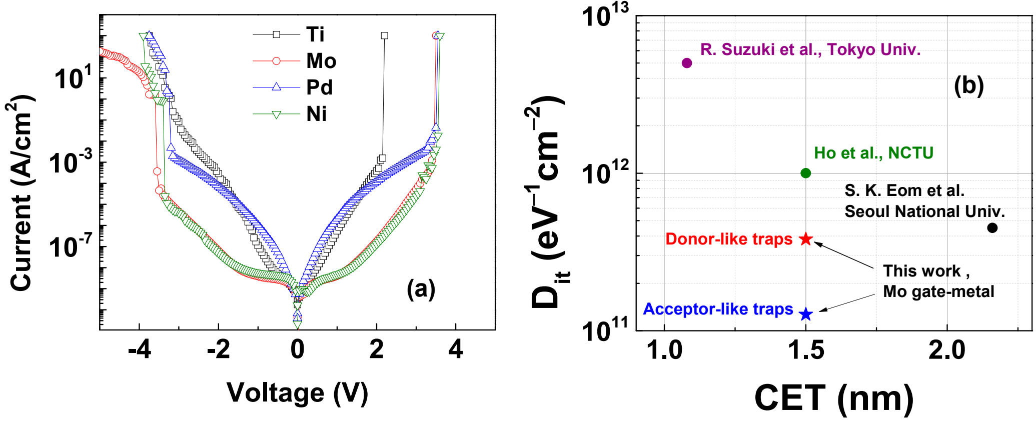

Figure 7. (**a**) I-V characteristics of M/HfO_2 MOSCAPS, M = Ti, Mo, Pd, Ni. (**b**) Benchmark of D_{it} as a function of CET of Mo/HfO_2/IGA MOSCAPs [2,59,60].

4. Conclusions

In summary, the impact of gate metals on interface traps and border traps in the metal/HfO_2/AlN/InGaAs structure was systematically studied. Due to oxidation at the metal/HfO_2 interface, low work function metal Ti creates the highest N_{BT} in HfO_2, while the middle work function metal Mo induces the lowest D_{it} and N_{BT}. The TCAD simulations confirm the occupation of traps around the CNL, where donor-like traps are ionized above CNL and acceptor-like traps are ionized below this level. The extracted lifetime of interface and border traps in this study are 2.9×10^{-9} s and 2.9×10^{-5} s, respectively. Interface traps distort the C-V characteristics, whereas border traps cause their hysteresis. The Heiman method was utilized to investigate the border traps in HfO_2. The lowest D_{it} and N_{BT} were found to be 1.39×10^{11} $eV^{-1}cm^{-2}$ and 4.46×10^{19} $eV^{-1}cm^{-3}$, respectively, for middle work function metal Mo due to a stable interface observed in XPS as well as a flat band voltage of 0 V. The results of this study provide guidance in the choice of gate metal for microelectronic devices and random-access memory.

Supplementary Materials: The following supporting information can be downloaded at https://www.mdpi.com/article/10.3390/mi14081606/s1, Figure S1: flow chart of process simulation in Silvaco TCAD to study the effects of interface and border traps in metal/HfO2/AlON/IGA structures.; Figure S2: TEM cross sections of metal/HfO_2/AlON/IGA structures. Metal: (a) Ti, (b) Mo, (c) Pd, (d) Ni. The Mo/HfO_2 and Ni/HfO_2 interfaces were found to have no interdiffusion, while the oxidation was observed at Ti/HfO_2 interface for Ti sample (indicated by white arrows). White arrows in Figure S2(c) demonstrate that Pd gate metal induces many defects in AlON passivation layer.

Author Contributions: Investigation, H.-B.D., Q.-H.L., P.V.P., A.-V.P.-G., T.-S.N., H.-M.L. and M.M.D.S.; formal analysis, H.-B.D.; conceptualization, H.-B.D.; writing—review and editing, H.-B.D., Q.-H.L., P.V.P., A.-V.P.-G., T.-S.N., H.-M.L. and M.M.D.S.; funding acquisition, H.-B.D.; supervision, H.-B.D. All authors have read and agreed to the published version of the manuscript.

Funding: This work was funded by the Ho Chi Minh City University of Technology and Education, Vietnam (grant No. T2022-29).

Institutional Review Board Statement: Not applicable

Informed Consent Statement: Not applicable

Data Availability Statement: The data that support the findings of this study are available from the corresponding author upon reasonable request.

Conflicts of Interest: The authors declare no conflict of interest.

References

1. Luc, Q.H.; Do, H.B.; Ha, M.T.H.; Hu, C.C.; Lin, Y.C.; Chang, E.Y. Plasma Enhanced Atomic Layer Deposition Passivated HfO_2/AlN/$In_{0.53}Ga_{0.47}As$ MOSCAPs with Sub-Nanometer Equivalent Oxide Thickness and Low Interface Trap Density. *IEEE Electron Device Lett.* **2015**, *36*, 1277–1280. [CrossRef]
2. Luc, Q.H.; Cheng, S.P.; Chang, P.C.; Do, H.B.; Chen, J.H.; Ha, M.T.H.; Huynh, S.H.; Hu, C.C.; Lin, Y.C.; Chang, E.Y. Effects of In-Situ Plasma-Enhanced Atomic Layer Deposition Treatment on the Performance of HfO_2/$In_{0.53}Ga_{0.47}As$ Metal–Oxide–Semiconductor Field-Effect Transistors. *IEEE Electron Device Lett.* **2016**, *37*, 974–977. [CrossRef]
3. Do, H.B.; Luc, Q.H.; Ha, M.T.H.; Hu, C.C.; Lin, Y.C.; Chang, E.Y. Impact of AlN Interfacial Dipole on Effective Work Function of Ni and Band Alignment of Ni/HfO_2/$In_{0.53}Ga_{0.47}As$ Gate-Stack. *IEEE Trans. Electron Devices* **2015**, *62*, 3987–3991. [CrossRef]
4. Do, H.B.; Luc, Q.H.; Ha, M.T.H.; Huynh, S.H.; Nguyen, T.A.; Hu, C.; Lin, Y.C.; Chang, E.Y. Investigation of Mo/Ti/AlN/HfO_2 High-k Metal Gate Stack for Low Power Consumption InGaAs NMOS Device Application. *IEEE Electron Device Lett.* **2017**, *38*, 552–555. [CrossRef]
5. Luc, Q.H.; Fan-Chiang, C.C.; Huynh, S.H.; Huang, P.; Do, H.B.; Ha, M.T.H.; Jin, Y.D.; Nguyen, T.A.; Zhang, K.Y.; Wang, H.C.; et al. First Experimental Demonstration of Negative Capacitance InGaAs MOSFETs with $Hf_{0.5}Zr_{0.5}O_2$ Ferroelectric Gate Stack. In Proceedings of the 2018 IEEE Symposium on VLSI Technology, Honolulu, HI, USA, 18–22 June 2018.
6. Song, T.; Tan, H.; Estandía, S.; Gàzquez, J.; Gich, M.; Dix, N.; Fina, I.; Sánchez, F. Improved polarization and endurance in ferroelectric $Hf_{0.5}Zr_{0.5}O_2$ films on $SrTiO_3$. *Nanoscale* **2022**, *14*, 2337–2343. [CrossRef]
7. Wan, J.; Chen, X.; Ji, L.; Tu, Z.; Wu, H.; Liu, C. Ferroelectricity of $Hf_{0.5}Zr_{0.5}O_2$ Thin Films Free from the Influence of Electrodes by Using Al_2O_3 Capping Layers. *IEEE Trans. Electron Devices* **2022**, *69*, 1805–1810. [CrossRef]
8. Wang, H.; Liu, J.; Wei, J.; Xiao, K.; Chen, Y.; Jiang, Y.-L.; Wan, J. Au Nanoparticles/HfO_2/Fully Depleted Silicon-on-Insulator MOSFET Enabled Rapid Detection of Zeptomole COVID-19 Gene with Electrostatic Enrichment Process. *IEEE Trans. Electron Devices* **2023**, *70*, 1236–1242. [CrossRef] [PubMed]
9. Das, S.K.; Chettri, B.; Karki, P.; Chettri, P.; Deka, U.; Sharma, B. Analysis of certain electrical properties in Silicon nanowire field-effect transistors with high-κ HfO_2 as gate dielectrics. In Proceedings of the 2022 IEEE International Conference of Electron Devices Society Kolkata Chapter (EDKCON), Kolkata, India, 26–27 November 2022.
10. Ram, M.S.; Svensson, J.; Skog, S.; Johannesson, S.; Wernersson, L.-E. Low-Frequency Noise in Vertical InAs/InGaAs Gate-All-Around MOSFETs at 15 K for Cryogenic Applications. *IEEE Electron Device Lett.* **2022**, *43*, 2033–2036. [CrossRef]
11. Liu, C.; Wang, Z.; Zhang, Y.; Lü, H.; Zhang, Y.M. Nanolaminated HfO_2/Al_2O_3 Dielectrics for High-Performance Silicon Nanomembrane Based Field-Effect Transistors on Biodegradable Substrates. *Adv. Mater. Interfaces* **2022**, *9*, 2201477.
12. Kumar, P.; Koley, K.; Goswami, R.; Maurya, A.; Kumar, S. Electrical Noise Behaviour of High-k Gate-All-Around MOSFET Based on Two-Port Device Network Analysis. In Proceedings of the 2022 14th International Conference on Information Technology and Electrical Engineering (ICITEE), Changsha, China, 4–6 November 2022.
13. Kumar, P.; Vashishath, M.; Gupta, N.; Gupta, R. High-k Dielectric Double Gate Junctionless (DG-JL) MOSFET for Ultra Low Power Applications- Analytical Model. *Silicon* **2022**, *14*, 7725–7734. [CrossRef]
14. Takagi, K.; Ono, T. First-principles study on leakage current caused by oxygen vacancies at HfO_2/SiO_2/Si interface. *Jpn. J. Appl. Phys.* **2018**, *57*, 066501. [CrossRef]
15. Do, H.B.; Luc, Q.H.; Ha, M.T.H.; Huynh, S.H.; Nguyen, T.A.; Lin, Y.C.; Chang, E.Y. Study of the interface stability of the metal (Mo, Ni, Pd)/HfO_2/AlN/InGaAs MOS devices. *AIP Adv.* **2017**, *7*, 085208. [CrossRef]
16. Zaffora, A.; Macaluso, R.; Habazaki, H.; Valov, I.; Santamaria, M. Electrochemically prepared oxides for resistive switching devices. *Electrochim. Acta* **2018**, *274*, 103–111. [CrossRef]
17. Kim, S.J.; Mohan, J.; Summerfelt, S.R.; Kim, J. Ferroelectric $Hf_{0.5}Zr_{0.5}O_2$ Thin Films: A Review of Recent Advances. *JOM* **2019**, *71*, 246–255. [CrossRef]
18. Chen, Y.Y.; Goux, L.; Clima, S.; Govoreanu, B.; Degraeve, R.; Kar, G.S.; Fantini, A.; Groeseneken, G.; Wouters, D.J.; Jurczak, M. Endurance/Retention Trade-off on HfO_2/Metal Cap 1T1R Bipolar RRAM. *IEEE Trans. Electron Devices* **2013**, *60*, 1114–1121. [CrossRef]
19. Dirkmann, S.; Kaiser, J.; Wenger, C.; Mussenbrock, T. Filament Growth and Resistive Switching in Hafnium Oxide Memristive Devices. *ACS Appl. Mater. Interfaces* **2018**, *10*, 14857–14868. [CrossRef]
20. Petzold, S.; Miranda, E.; Sharath, S.U.; Muñoz-Gorriz, J.; Vogel, T.; Piros, E.; Kaiser, N.; Eilhardt, R.; Zintler, A.; Molina-Luna, L.; et al. Analysis and simulation of the multiple resistive switching modes occurring in HfOx-based resistive random access memories using memdiodes. *J. Appl. Phys.* **2019**, *125*, 234503. [CrossRef]

21. Cheynet, M.C.; Pokrant, S.; Tichelaar, F.D.; Rouvière, J.-L. Crystal structure and band gap determination of HfO_2 thin films. *J. Appl. Phys.* **2007**, *101*, 054101. [CrossRef]
22. Rushchanskii, K.Z.; Blügel, S.; Ležaić, M. Routes for increasing endurance and retention in HfO_2-based resistive switching memories. *Phys. Rev. Mater.* **2018**, *2*, 115002. [CrossRef]
23. Xue, K.H.; Blaise, P.; Fonseca, L.R.; Nishi, Y. Prediction of Semimetallic Tetragonal Hf_2O_3 and Zr_2O_3 from First Principles. *Phys. Rev. Lett.* **2013**, *110*, 065502. [CrossRef] [PubMed]
24. Rushchanskii, K.Z.; Blügel, S.; Ležaić, M. Ab initio phase diagrams of Hf–O, Zr–O and Y–O: A comparative study. *Faraday Discuss.* **2019**, *213*, 321–337. [CrossRef] [PubMed]
25. Vais, A.; Alian, A.; Nyns, L.; Franco, J.; Sioncke, S.; Putcha, V.; Yu, H.; Mols, Y.; Rooyackers, R.; Lin, D.; et al. Record mobility (μeff ~3100 cm2/V-s) and reliability performance (Vov ~0.5 V for 10 yr operation) of In0.53Ga0.47As MOS devices using improved surface preparation and a novel interfacial layer. In Proceedings of the 2016 IEEE Symposium on VLSI Technology, Honolulu, HI, USA, 14–16 June 2016.
26. Lin, J.; Zhao, X.; Clavero, I.M.; Antoniadis, D.A.; del Alamo, J.A. A Scaling Study of Excess off-State Current in InGaAs Quantum-Well MOSFETs. *IEEE Trans. Electron Devices* **2019**, *66*, 1208–1212. [CrossRef]
27. Cai, X.; Vardi, A.; Grajal, J.; del Alamo, J.A. Reassessing InGaAs for Logic: Mobility Extraction in sub-10 nm Fin-Width FinFETs. In Proceedings of the 2019 Symposium on VLSI Technology, Kyoto, Japan, 9–14 June 2019.
28. Ko, H.-L.; Luc, Q.H.; Huang, P.; Wu, J.-Y.; Chen, S.-M.; Tran, N.-A.; Hsu, H.-T.; Chang, E.Y. Sub-10 nm Top Width Nanowire InGaAs Gate-All-Around MOSFETs with Improved Subthreshold Characteristics and Device Reliability. *IEEE J. Electron Devices Soc.* **2022**, *10*, 188–191. [CrossRef]
29. Cai, X.; Vardi, A.; Grajal, J.; del Alamo, J.A. A New Technique for Mobility Extraction in MOSFETs in the Presence of Prominent Gate Oxide Trapping: Application to InGaAs MOSFETs. *IEEE Trans. Electron Devices* **2020**, *67*, 3075–3081. [CrossRef]
30. Pallecchi, I.; Grassano, G.; Marré, D.; Pellegrino, L.; Putti, M.; Siri, A.S. $SrTiO_3$-based metal–insulator–semiconductor heterostructures. *Appl. Phys. Lett.* **2001**, *78*, 2244–2246. [CrossRef]
31. Xuan, Y.; Wu, Y.Q.; Shen, T.; Yang, T.; Ye, P.D. High performance submicron inversion-type enhancement-mode InGaAs MOSFETs with ALD Al_2O_3, HfO_2 and HfAlO as gate dielectrics. In Proceedings of the 2007 IEEE International Electron Devices Meeting, Washington, DC, USA, 10–12 December 2007.
32. Putcha, V.; Franco, J.; Vais, A.; Kaczer, B.; Xie, Q.; Maes, J.W.; Tang, F.; Givens, M.; Collaert, N.; Linten, D.; et al. Extensive assessment of the charge-trapping kinetics in InGaAs MOS gate-stacks for the demonstration of improved BTI reliability. *Microelectron. Reliab.* **2020**, *115*, 113996. [CrossRef]
33. Li, Y.; Deng, S.; Li, J.; Li, G.; Zhang, S.; Jin, Y. Investigation on HfO_2 properties grown by ALD using TDMAH as precursor. *Vacuum* **2022**, *203*, 111243. [CrossRef]
34. Robertson, J. High dielectric constant oxides. *Eur. Phys. J. Appl. Phys.* **2004**, *28*, 265–291. [CrossRef]
35. Yeo, Y.-C.; King, T.-J.; Hu, C. Direct tunneling leakage current and scalability of alternative gate dielectrics. *Appl. Phys. Lett.* **2002**, *81*, 2091–2093. [CrossRef]
36. Michaelson, H.B. The work function of the elements and its periodicity. *J. Appl. Phys.* **2008**, *48*, 4729–4733. [CrossRef]
37. Stemmer, S.; Chobpattana, V.; Rajan, S. Frequency dispersion in III–V metal-oxide-semiconductor capacitors. *Appl. Phys. Lett.* **2012**, *100*, 233510. [CrossRef]
38. Ji, Z.; Zhang, X.; Franco, J.; Gao, R.; Duan, M.; Zhang, J.F.; Zhang, W.D.; Kaczer, B.; Alian, A.; Linten, D.; et al. An Investigation on Border Traps in III–V MOSFETs with an $In_{0.53}Ga_{0.47}As$ Channel. *IEEE Trans. Electron Devices* **2015**, *62*, 3633–3639. [CrossRef]
39. Sicre, S.B.F.; Souza, M.M.D. Analysis of P_b Centers in Ultrathin Hafnium Silicate Gate Stacks. *IEEE Trans. Electron Devices* **2007**, *54*, 2551–2555. [CrossRef]
40. Chang, Y.C.; Huang, M.L.; Lee, K.Y.; Lee, Y.J.; Lin, T.D.; Hong, M.; Kwo, J.; Lay, T.S.; Liao, C.C.; Cheng, K.Y. Atomic-layer-deposited HfO_2 on $In_{0.53}Ga_{0.47}As$: Passivation and energy-band parameters. *Appl. Phys. Lett.* **2008**, *92*, 072901. [CrossRef]
41. Sune, J.; Olivo, P.; Ricco, B. Quantum-mechanical modeling of accumulation layers in MOS structure. *IEEE Trans. Electron Devices* **1992**, *39*, 1732–1739. [CrossRef]
42. Park, P.K.; Kang, S.-W. Enhancement of dielectric constant in HfO_2 thin films by the addition of Al_2O_3. *Appl. Phys. Lett.* **2006**, *89*, 192905. [CrossRef]
43. Madelung, O.; Rössler, U.; Schulz, M. (Eds.) PdO: Optical properties, dielectric constant: Datasheet from Landolt-Börnstein—Group III Condensed Matter. In *Non-Tetrahedrally Bonded Binary Compounds II*; SpringerMaterials; Springer: Berlin/Heidelberg, Germany, 2000; Volume 41D. [CrossRef]
44. Kim, H.; Chavan, V.D.; Aziz, J.; Ko, B.; Lee, J.-S.; Rho, J.; Dongale, T.D.; Choi, K.-K.; Kim, D.-K. Effect of ALD Processes on Physical and Electrical Properties of HfO_2 Dielectrics for the Surface Passivation of a CMOS Image Sensor Application. *IEEE Access* **2022**, *10*, 68724–68730. [CrossRef]
45. Palumbo, F.; Krylov, I.; Eizenberg, M. Comparison of the degradation characteristics of AlON/InGaAs and Al_2O_3/InGaAs stacks. *J. Appl. Phys.* **2015**, *117*, 104103. [CrossRef]
46. Choi, M.; Lyons, J.L.; Janotti, A.; Van de Walle, C.G. Impact of carbon and nitrogen impurities in high-κ dielectrics on metal-oxide-semiconductor devices. *Appl. Phys. Lett.* **2013**, *102*, 142902. [CrossRef]
47. Engel-Herbert, R.; Hwang, Y.; Stemmer, S. Comparison of methods to quantify interface trap densities at dielectric/III–V semiconductor interfaces. *J. Appl. Phys.* **2010**, *108*, 124101. [CrossRef]

48. Ahrenkiel, R.K.; Ellingson, R.; Johnston, S.; Wanlass, M. Recombination lifetime of $In_{0.53}Ga_{0.47}As$ as a function of doping density. *Appl. Phys. Lett.* **1998**, *72*, 3470–3472. [CrossRef]
49. Roll, G.; Mo, J.; Lind, E.; Johansson, S.; Wernersson, L.-E. Defect evaluation in InGaAs field effect transistors with HfO_2 or Al_2O_3 dielectric. *Appl. Phys. Lett.* **2015**, *106*, 203503. [CrossRef]
50. Heiman, F.P.; Warfield, G. The effects of oxide traps on the MOS capacitance. *IEEE Trans. Electron Devices* **1965**, *12*, 167–178. [CrossRef]
51. Zhang, X.-Y.; Hsu, C.-H.; Cho, Y.-S.; Lien, S.-Y.; Zhu, W.-Z.; Chen, S.-Y.; Huang, W.; Xie, L.-G.; Chen, L.-D.; Zou, X.-Y.; et al. Simulation and Fabrication of HfO_2 Thin Films Passivating Si from a Numerical Computer and Remote Plasma ALD. *Appl. Sci.* **2017**, *7*, 1244. [CrossRef]
52. Xia, H.; Li, T.-X.; Tang, H.-J.; Zhu, L.; Li, X.; Gong, H.-M.; Lu, W. Nanoscale imaging of the photoresponse in PN junctions of InGaAs infrared detector. *Sci. Rep.* **2016**, *6*, 21544. [CrossRef] [PubMed]
53. Winter, R.; Krylov, I.; Ahn, J.; McIntyre, P.C.; Eizenberg, M. The effect of post oxide deposition annealing on the effective work function in metal/Al_2O_3/InGaAs gate stack. *Appl. Phys. Lett.* **2014**, *104*, 202103. [CrossRef]
54. Das, T.; Mahata, C.; Maiti, C.K.; Miranda, E.; Sutradhar, G.; Bose, P.K. Effects of Ti incorporation on the interface properties and band alignment of HfTaOx thin films on sulfur passivated GaAs. *Appl. Phys. Lett.* **2011**, *98*, 022901. [CrossRef]
55. Sanchez-Martinez, A.; Ceballos-Sanchez, O.; Vazquez-Lepe, M.O.; Duong, T.; Arroyave, R.; Espinosa-Magaña, F.; Herrera-Gomez, A. Diffusion of In and Ga in TiN/HfO_2/InGaAs nanofilms. *J. Appl. Phys.* **2013**, *114*, 143504. [CrossRef]
56. Application Note. *Characterization of High-k Dielectric Materials on Silicon Using Angle Resolved XPS*; Thermo Fisher Scientific Inc.: Bartlesville, OK, USA, 2008.
57. Yoshida, S.; Lin, D.; Vais, A.; Alian, A.; Franco, J.; El Kazzi, S.; Mols, Y.; Miyanami, Y.; Nakazawa, M.; Collaert, N.; et al. Systematic study of interfacial reactions induced by metal electrodes in high-k/InGaAs gate stacks. *Appl. Phys. Lett.* **2016**, *109*, 172101. [CrossRef]
58. Olivo, P.; Sune, J.; Ricco, B. Determination of the Si-SiO_2/barrier height from the Fowler-Nordheim plot. *IEEE Electron Device Lett.* **1991**, *12*, 620–622. [CrossRef]
59. Suzuki, R.; Taoka, N.; Yokoyama, M.; Lee, S.; Kim, S.H.; Hoshii, T.; Yasuda, T.; Jevasuwan, W.; Maeda, T.; Ichikawa, O.; et al. 1-nm-capacitance-equivalent-thickness HfO_2/Al_2O_3/InGaAs metal-oxide-semiconductor structure with low interface trap density and low gate leakage current density. *Appl. Phys. Lett.* **2012**, *100*, 132906. [CrossRef]
60. Eom, S.-K.; Kong, M.-W.; Kang, M.-J.; Lee, J.-G.; Cha, H.-Y.; Seo, K.-S. Enhanced Interface Characteristics of PA-ALD HfOxNy/InGaAs MOSCAPs Using IPA Oxygen Reactant and Cyclic N_2 Plasma. *IEEE Electron Device Lett.* **2018**, *39*, 1636–1639. [CrossRef]

Disclaimer/Publisher's Note: The statements, opinions and data contained in all publications are solely those of the individual author(s) and contributor(s) and not of MDPI and/or the editor(s). MDPI and/or the editor(s) disclaim responsibility for any injury to people or property resulting from any ideas, methods, instructions or products referred to in the content.